Electronic Supplementary Information (ESI) for Energy & Environmental Science.

Supporting Information

Multifunctional Additive with Dynamic Sacrificial S-S Bond for Building Self-assembled Monolayers of Zn-Ion Battery with Improved Stability and Longevity

*Shuang Han,[a] Minghai Li,[a] Qiyu Fan,[a] Zhuoyi Han,[a] Xuewen Ming,[a] Wen Wang,[b] Wanan Cai *[a] and Haijun Niu *[a]*

[a] Key Laboratory of Functional Inorganic Material, Ministry of Education, Department of Macromolecular Materials and Engineering, School of Chemical, Chemical Engineering and Materials, Heilongjiang University, Harbin 150086, PR China.

[b] School of Materials Science and Engineering, Harbin Institute of Technology, Harbin 150080, PR China.

* Corresponding author: haijunniu@hotmail.com, caiwanan@hlju.edu.cn.

Experimental Section

1. Chemicals and Materials

Zinc sulfate heptahydrate ($ZnSO_4 \cdot 7H_2O$, AR, >99.5%), ammonium metavanadate (NH_4VO_3, AR, ≥99.0%), ethanedioic acid dihydrate ($H_2C_2O_4 \cdot 2H_2O$, AR, ≥99.5%) were purchased from Sinopharm Chemical Reagent Co., Ltd. *Bis*(*2*-hydroxyethyl) disulfide

(BHED, ≥98%), *1*-methyl-*2*-pyrrolidinone (NMP, AR, ≥99%) were purchased from Aladdin. Super P carbon (99.9%), polyvinylidene fluoride (PVDF, ≥99.5%) and glass fiber filters (Whatman, GF/D) were purchased from Guangdong Canrd New Energy Technology Co., Ltd. Zn foils (99.99%, 100 μm and 10 μm thickness), Cu foils (99.8%, 15 μm thickness), Ti foils (99.9%, 20 μm thickness), stainless steel mesh (400 mesh) were purchased from Tianjin Aiweixin Chemical Technology Co., Ltd.

2. Electrolyte preparation

2M $ZnSO_4$ electrolyte was prepared by dissolving $ZnSO_4 \cdot 7H_2O$ in deionized water at room temperature. The control electrolytes were prepared by adding BHED additives at varying concentrations (2, 4, 6, and 8 mM, respectively) to a 2M $ZnSO_4$ electrolyte. The optimal concentration of BHED was 2M $ZnSO_4$ + 4 mM BHED, and this was denoted as $ZnSO_4$ + BHED electrolyte.

3. Preparation of $NH_4V_4O_{10}$ cathode

$NH_4V_4O_{10}$ (NVO) was synthesized according to the reference.[1] Typically, 5 mmol NH_4VO_3 and 5 mmol $H_2C_2O_4 \cdot 2H_2O$ were dissolved in 75 mL of deionized water and stirred for 1 hour. The mixture was then transferred to a 100 mL Teflon-lined stainless steel autoclave and maintained at 180 ℃ for 12 h. The product was obtained by centrifugation and washed several times with ethanol and deionized water. Finally, $NH_4V_4O_{10}$ samples are obtained by vacuum drying at 60 ℃ for 12 h. For the NVO cathodes, a slurry mixed by NVO, Super P carbon, and PVDF at a weight ratio of 7:2:1 in NMP solvent was coated on Ti foils and stainless steel and dried under vacuum at 80 ℃ for 12 h. The mass loading of active material on the electrode is 1.2 ~ 1.5 mg cm^{-2}

for the button cells and 6 ~ 9 mg cm^{-2} for the flexible batteries.

4. Materials characterization

The fundamental properties of the electrolyte are tested by the pH meter, conductivity meter and Ubbelohde Viscometer. ^1H nuclear magnetic resonance (^1H NMR, Bruker-400 MHz using D_2O as the solvent) spectra and Fourier transform infrared (FTIR, PerkinElmer Spectrum 100) spectra were used to probe the effect of BHED upon the solvation structure of Zn^{2+}. The contact angles of $ZnSO_4$ electrolytes with different BHED contents on Zn foils were tested by a JC20001 contact angle goniometer. The phase structures of the samples were studied by X-ray diffraction spectroscopy (XRD, Rigaku D/max 2500) with a Cu K_α X-ray source, scanning the angular range (2θ) from 5° to 80°. Field emission scanning electron microscopy (FESEM, Hitachi S-4800, Japan) and atomic force microscopy (AFM, Agilent, SPM5100) were employed to investigate the surface morphologies and microstructure of the samples. The Zn^{2+} deposition process on the Zn electrode surface was monitored using a Metallurgical Microscope 9XB-PC (Shanghai Optical Instrument Factory) and a custom in-situ reaction cell which is composed of a PTFE electrolytic cell and two Zn foil electrodes. The surface chemical state and composition were analyzed using XPS (Kratos AXIS Ultra DLD) with an Al K_α X-ray source. Data were processed with CasaXPS software, and all spectra were calibrated to the C 1s line at 284.8 eV as an internal reference. Raman spectroscopy (HORIBA Jobin Yvo) was carried out by a confocal photoprobe with a 633 nm laser beam. The Zn||Zn symmetric cells were connected with the Neware test system, and the outlet gas was finally flowed into the

DEMS instrument (QMG220, Linglu Instrument (Shanghai) Co. Ltd).

5. Electrochemical evaluation

The Zn||Zn symmetric cells, the Zn||Cu asymmetric cells, the Zn||Ti asymmetric cells, and the Zn||NVO full cells were assembled in air to form the coin cells (CR2032). Galvanostatic cycling, overpotential curves, self-discharge test, and rate capability tests were conducted with a multichannel cell test system (Neware CT-4008Tn-5V50mA, Shenzhen, China) at room temperature. The cyclic voltammetry (CV) and electrochemical impedance spectroscopy (EIS), linear scanning voltammetry (LSV), Tafel profiles, Zn^{2+} transfer number ($t_{Zn^{2+}}$), chronoamperometry (CA) and activation energy (E_a) were recorded using a CHI 660E electrochemical workstation. LSV tests were measured using the Zn||Ti asymmetric cells in a voltage window of -0.4 to 3 V at a scan rate of 5 mV s^{-1}. CA tests were conducted using the Zn||Zn symmetric cells under a bias voltage of -150 mV for 400 s.

The inhibitory efficiency calculation:

The corrosion potentials and current densities obtained from the Tafel curves for $ZnSO_4$ and $ZnSO_4$ + BHED electrolytes were listed in Table S1. The inhibitory efficiency (I) was further utilized to assess the impact of BHED on the corrosion resistance of the Zn electrode, calculated according to the following formula:

$$I = (j_{corr} - j'_{corr})/j_{corr} \qquad \text{Equation (S1)}$$

Where j_{corr} and j'_{corr} are the corrosion current density in $ZnSO_4$ and $ZnSO_4$ + BHED electrolytes, respectively.

The Zn^{2+} transfer number calculation:

The transference number of Zn^{2+} ($t_{Zn^{2+}}$) was evaluated by measuring the EIS of the Zn||Zn symmetric cells before and after the chronoamperometric (CA) tests, calculated using the formula below:

$$t_{Zn^{2+}} = \frac{I_s(\Delta V - I_0 R_0)}{I_0(\Delta V - I_s R_s)} \quad \text{Equation (S2)}$$

Where ΔV is the applied polarization potential (15 mV), I_0 and R_0 are the current and charge-transfer resistance at the initial state, respectively; and I_s and R_s are the current and charge-transfer resistance at the steady state, respectively.

The activation energy calculation:

Electrochemical impedance spectroscopy (EIS) data for the Zn||Zn symmetrical cells were collected at specific temperatures (30 °C, 40 °C, 50 °C, and 60 °C). The activation energy (E_a) was determined by fitting the obtained charge transfer resistance (R_{ct}) in accordance with the Arrhenius equation.

$$\frac{1}{R_{ct}} = A\ exp(-\frac{E_a}{RT}) \quad \text{Equation (S3)}$$

Where R_{ct} is the charge transfer resistance, A is the pre-exponential factor, E_a is the activation energy, R is the ideal gas constant, and T is the absolute temperature.

The exchange current density:

The nucleation overpotentials of the Zn||Cu asymmetric cells were collected at various current densities (0.5 ~ 3 mA cm^{-2}). The exchange current density (i_o) related to the Zn^{2+} deposition process was obtained according to the following equation:

$$i = i_0 \frac{F\ \eta}{RT2} \quad \text{Equation (S4)}$$

Where i is the running current density, i_o is and exchange current density, F is the

Faradaic constant, R is the ideal gas constant, T is the deposition temperature, and η is nucleation overpotential.

6. Density functional theory calculations

Binding energy, adsorption energy, molecular electrostatic potential (MESP), Highest Occupied Molecular Orbital (HOMO), and Lowest Unoccupied Molecular Orbital (LUMO) were all calculated using the Vienna Ab-initio Simulation Package (VASP) for the DFT calculation. VASPKIT was used in the representation of HOMO and LUMO, and the structure visualization was performed using VESTA. The charge density difference figure is obtained with the help of VASP and VASPKIT software.

The adsorption energy calculation:

The adsorption energy between Zn slab and molecular is defined by the following Equation:

$$E_{ad}(Zn + molecular) = E_{Zn\,+\,molecular} - E_{Zn} - E_{molecular} \qquad \text{Equation (S5)}$$

Where $E_{\mathrm{Zn+molecular}}$ is the energy of adsorption structure of Zn slab and adsorbed molecular, E_{Zn} is the energy of Zn slab and $E_{\mathrm{molecular}}$ is the energy of absorbed molecular.

The binding energy calculation:

The binding energy between molecular and Zn ion is defined by the following Equation:

$$E_b(molecular + ion) = E_{molecular\,+\,ion} - E_{molecular} - E_{ion} \qquad \text{Equation (S6)}$$

Where $E_{molecular+ion}$ is the energy of the bound structure of the molecular and Zn ion, $E_{molecular}$ is the energy of isolated molecular and E_{ion} is the energy of isolated Zn ion.

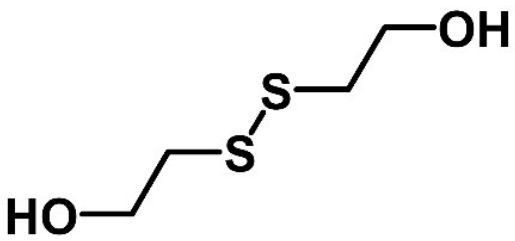

Figure S1. Schematic of the molecular formula of BHED.

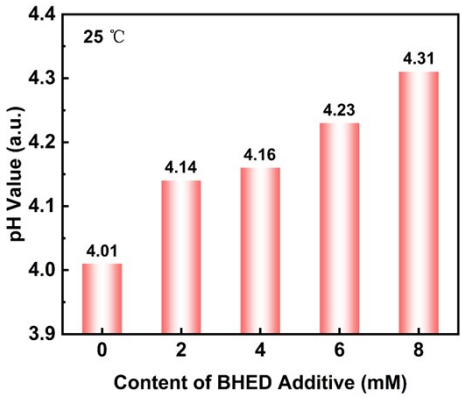

Figure S2. The pH values of $ZnSO_4$ electrolytes with various content of BHED additives.

The pH values of $ZnSO_4$ electrolyte with various content of BHED additives were measured using a calibrated pH meter at room temperature. The results showed that the pH values of the electrolyte increased significantly with the increase of BHED content. The increase in pH helps to inhibit hydrogen precipitation reaction (HER) and interfacial corrosion, which significantly improves the stability of the zinc anode.[2, 3]

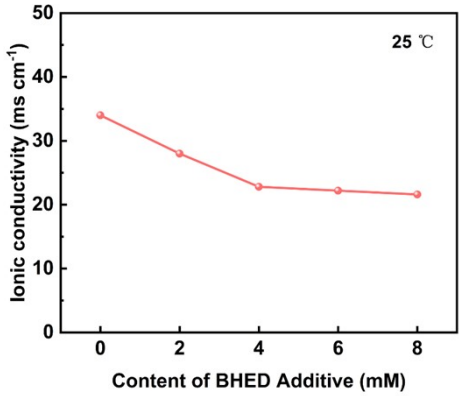

Figure S3. Ionic conductivity of $ZnSO_4$ electrolyte with various content of BHED additives.

The ionic conductivity of the 2M $ZnSO_4$ electrolyte was measured versus the concentration of BHED additive at 25 °C using a calibrated conductivity meter. Although the addition of BHED resulted in a slight decrease in the ionic conductivity of the electrolyte, it remained within the same order of magnitude. In addition, further increase in BHED concentration stabilizes the ionic conductivity, which ensures that the electrolyte still maintains high conductivity values in practical applications.[4, 5]

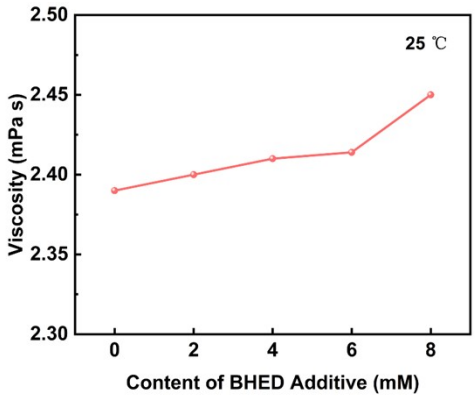

Figure S4. The viscosities of $ZnSO_4$ electrolyte with various content of BHED additives.

The relative viscosity of the electrolyte was determined by measuring the outflow time of the solution and pure solvent in the capillary tube at room temperature by means of an Ubbelohde Viscometer. The viscosity of the electrolyte increased with the addition of BHED. This is mainly attributed to the formation of strong interactions between BHED and H_2O molecules, leading to an increase in the overall viscosity of the electrolyte.[6]

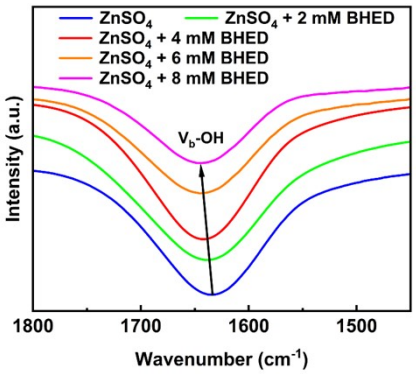

Figure S5. FTIR spectra in the range of 1800 ~ 1450 cm^{-1} of $ZnSO_4$ electrolytes with different BHED contents.

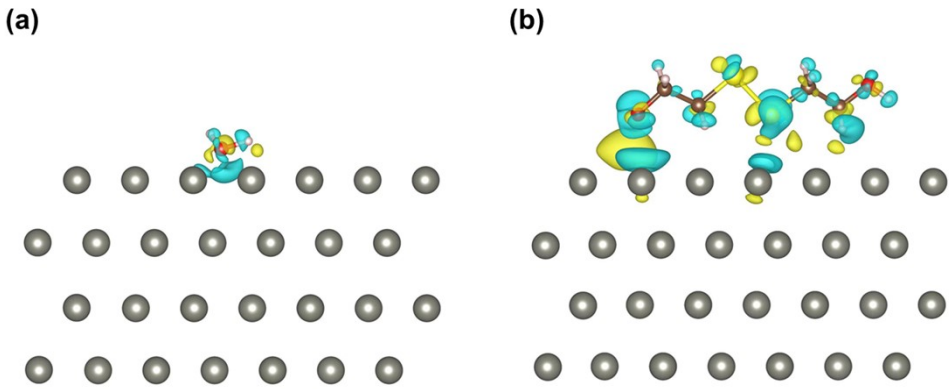

Figure S6. Differential charge density distribution of a) H_2O and b) BHED molecule

adsorbed on Zn slabs. Yellow (cyan) represents charge accumulation (deletion).

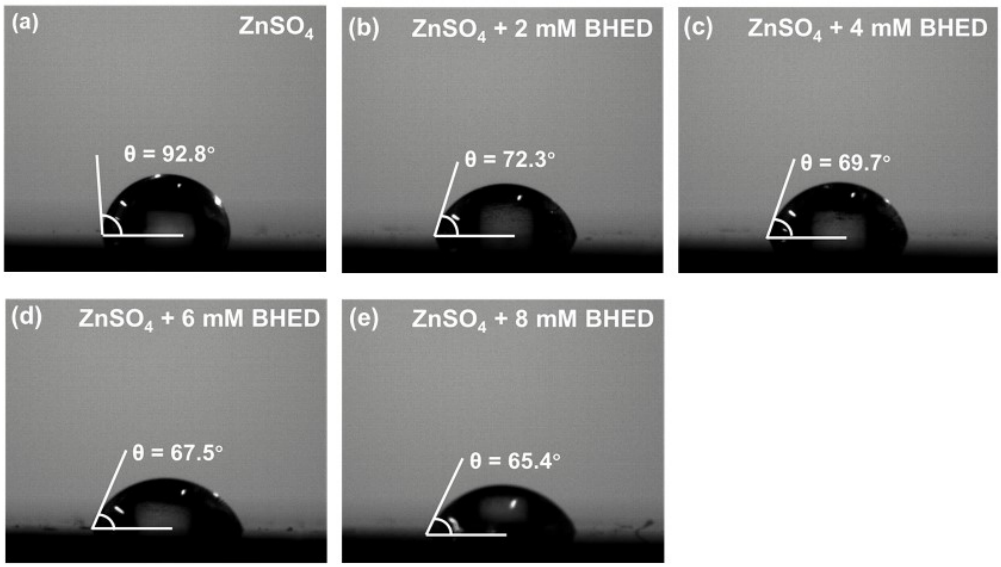

Figure S7. Optical photographs showing contact angles of a) $ZnSO_4$, b) $ZnSO_4$ + 2 mM BHED, c) $ZnSO_4$ + 4 mM BHED, d) $ZnSO_4$ + 6 mM BHED and e) $ZnSO_4$ + 8 mM BHED electrolytes on the Zn foil surface.

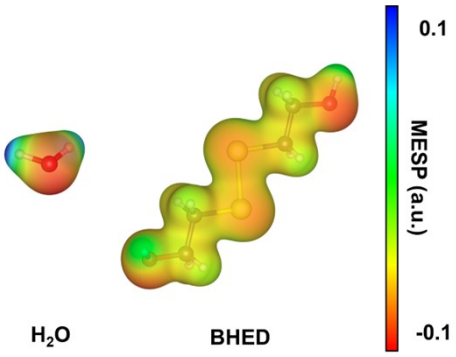

Figure S8. Molecular electrostatic potential (MESP) mapping of H_2O and BHED molecules.

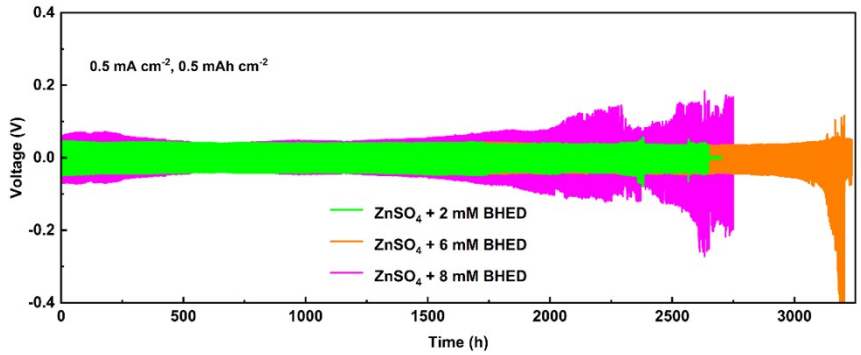

Figure S9. The voltage-time curves of the Zn||Zn symmetric cells in $ZnSO_4$ electrolytes with different BHED contents at 0.5 mA cm^{-2} and 0.5 mAh cm^{-2}.

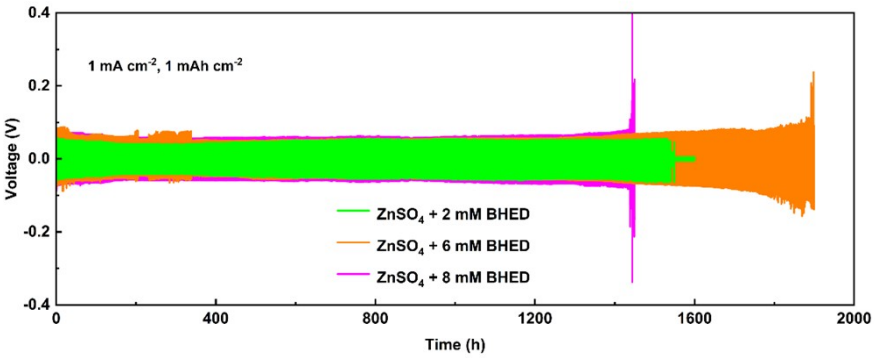

Figure S10. The voltage-time curves of the Zn||Zn symmetric cells in $ZnSO_4$ electrolytes with different BHED contents at 1 mA cm^{-2} and 1 mAh cm^{-2}.

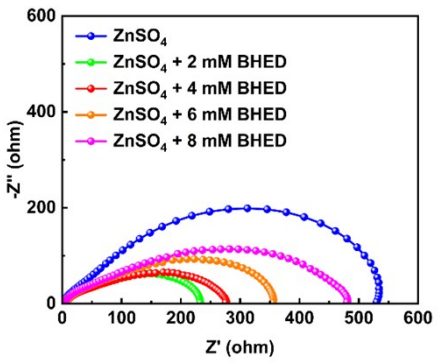

Figure S11. EIS plots of the Zn||Zn symmetrical cells in $ZnSO_4$ electrolytes with

different BHED contents.

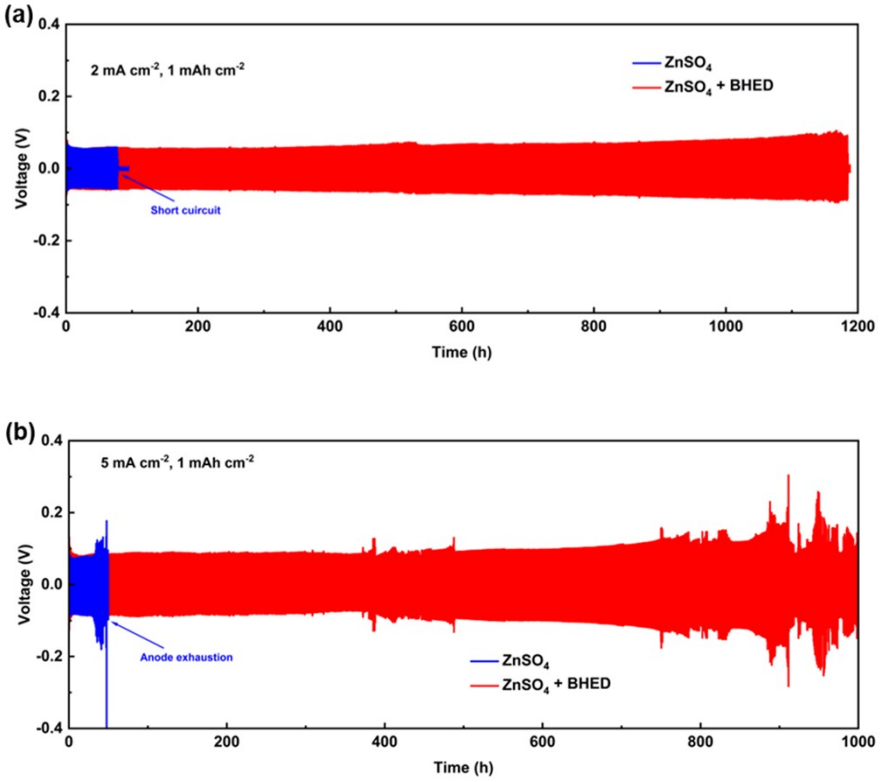

Figure S12. The voltage-time curves of the Zn||Zn symmetric cells in $ZnSO_4$ and $ZnSO_4$ + BHED electrolytes at a) 2 mA cm^{-2} and 1 mAh cm^{-2} and b) 5 mA cm^{-2} and 1 mAh cm^{-2}.

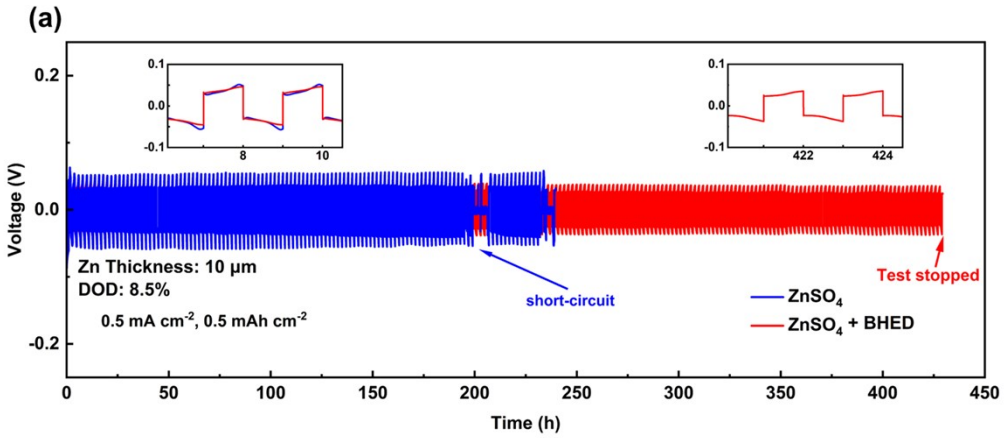

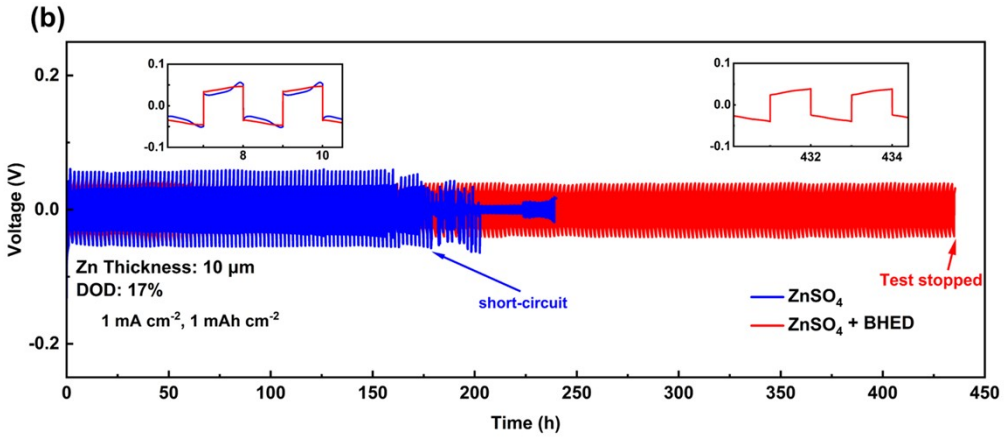

Fig S13. The voltage-time curves of the Zn||Zn symmetric cells in $ZnSO_4$ and $ZnSO_4$ + BHED electrolytes at a) 0.5 mA cm^{-2} and 0.5 mAh cm^{-2} and b) 1 mA cm^{-2} and 1 mAh cm^{-2} under the DOD of 8.5% and 17%. (The thickness of Zn foils is 10 μm, test stopped due to time constraints)

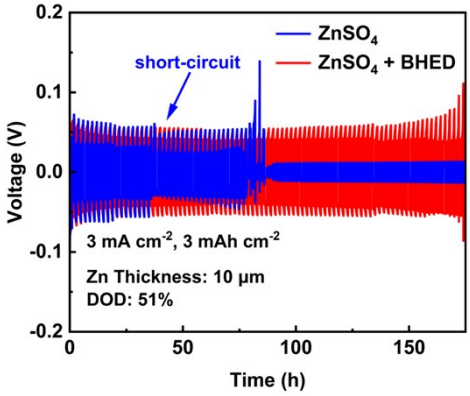

Figure S14. The voltage-time curves of the Zn||Zn symmetric cells in $ZnSO_4$ and $ZnSO_4$ + BHED electrolytes at 3 mA cm^{-2} and 3 mAh cm^{-2} under the DOD of 51%. (The thickness of Zn foils is 10 μm).

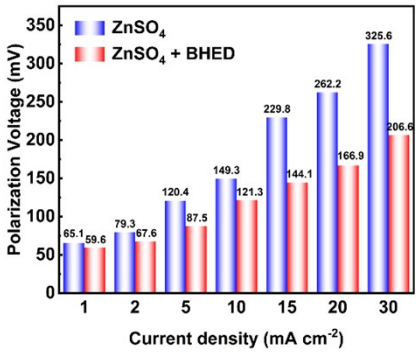

Figure S15. Voltage hysteresis of the Zn||Zn symmetrical cells in $ZnSO_4$ and $ZnSO_4$ + BHED electrolytes at a current density of 1 to 30 mA cm^{-2}.

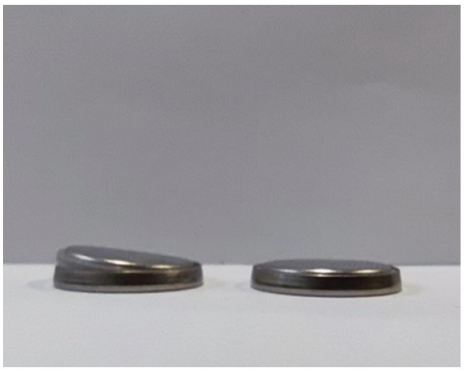

Figure S16. The state of the button cells after cycles in $ZnSO_4$ (left) and $ZnSO_4$ + BHED (right) electrolytes.

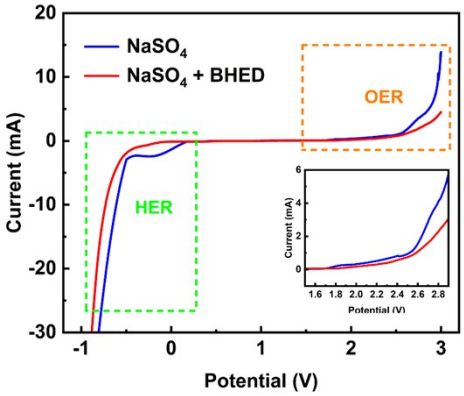

Figure S17. LSV curves for Zn electrodes in 2M Na_2SO_4 and 2M Na_2SO_4 + BHED

electrolytes.

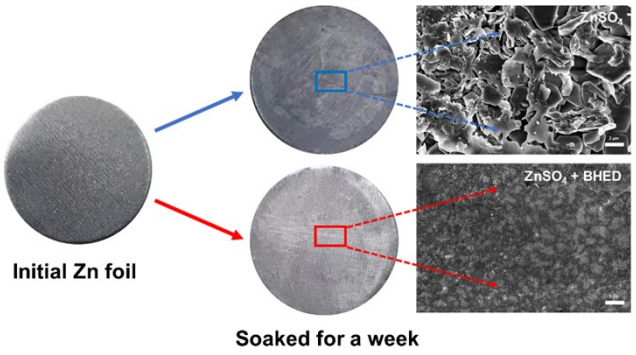

Figure S18. SEM images of Zn foil soaked for a week in $ZnSO_4$ and $ZnSO_4$ + BHED electrolytes.

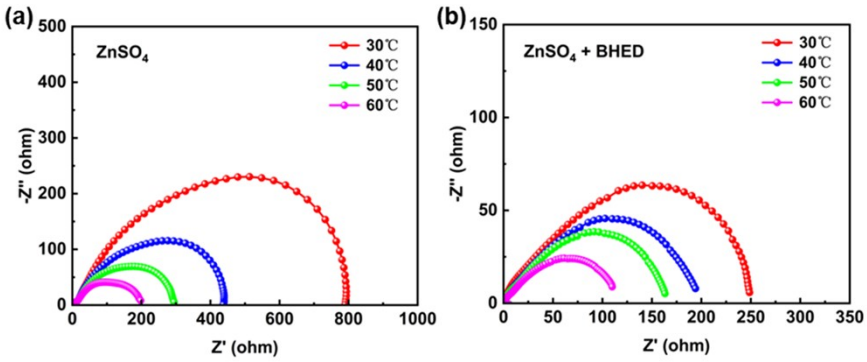

Figure S19. EIS plots of the Zn||Zn symmetrical cells in a) $ZnSO_4$ and b) $ZnSO_4$ + BHED electrolytes at different temperatures.

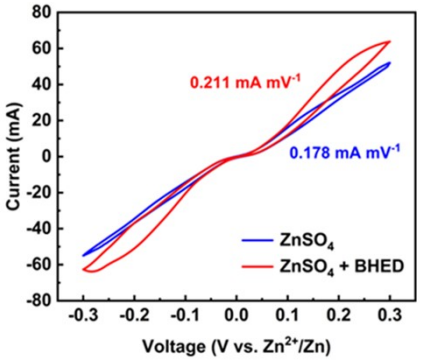

Figure S20. CV curves of the Zn||Zn symmetric cells in $ZnSO_4$ and $ZnSO_4$ + BHED electrolytes.

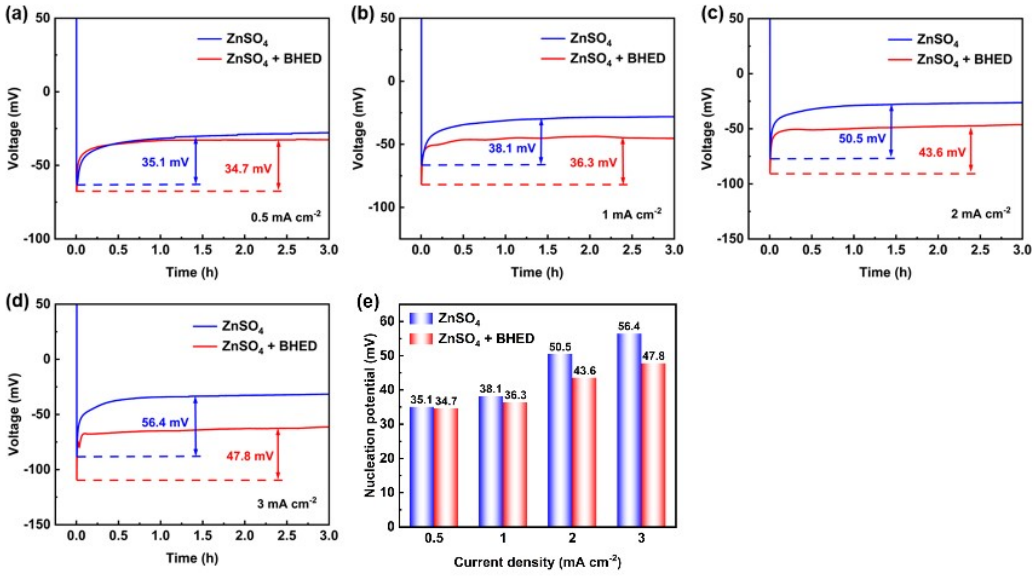

Figure S21. Zn^{2+} deposition curves on the Cu electrode in different electrolytes at current densities of a) 0.5 mA cm^{-2}, b) 1 mA cm^{-2}, c) 2 mA cm^{-2}, and d) 3 mA cm^{-2}. e) Comparison of nucleation overpotentials at different current densities in $ZnSO_4$ and $ZnSO_4$ + BHED electrolytes.

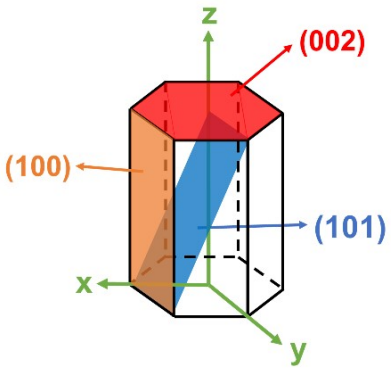

Figure S22. The illustration of the hexagonal close-packed structure of Zn.

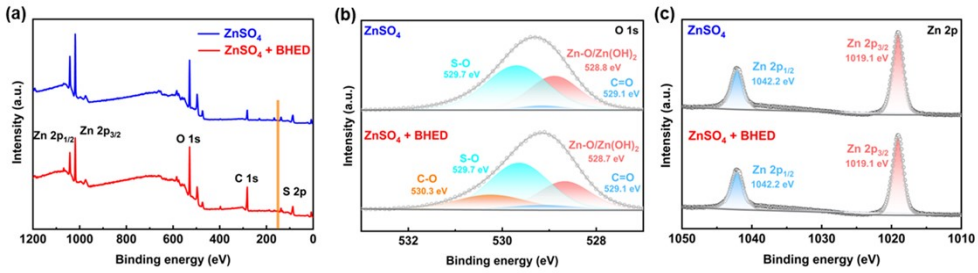

Figure S23. a) XPS survey, XPS spectrum of b) O 1s and c) Zn 2p for Zn electrodes after 30 cycles in different electrolytes at 0.5 mA cm^{-2} and 0.5 mAh cm^{-2}.

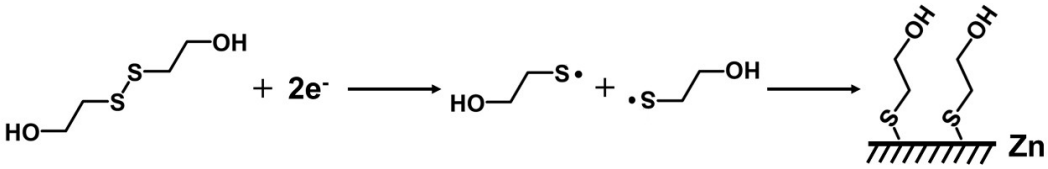

Figure S24. The possible decomposition pathways of BHED additive and their chemical reactions on the Zn metal surface during Zn^{2+} plating/stripping process.

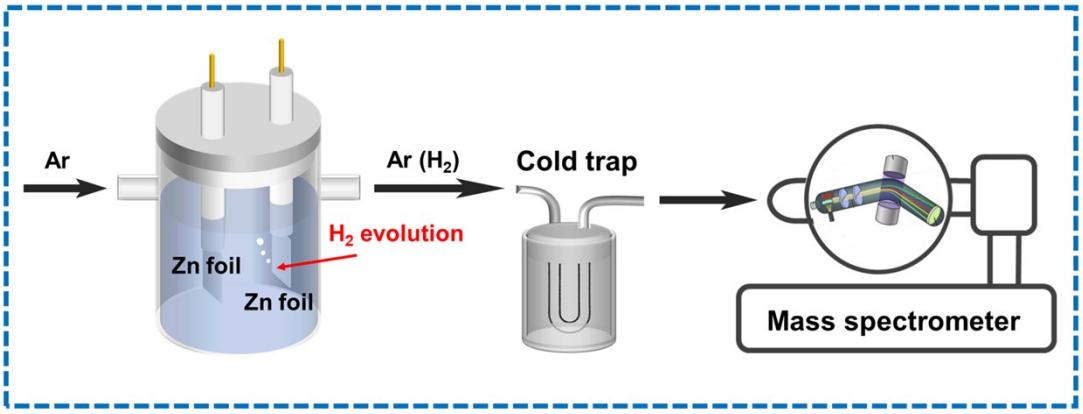

Figure S25. The schematic diagram of in-situ DEMS testing apparatus with an electrochemical reaction cell.

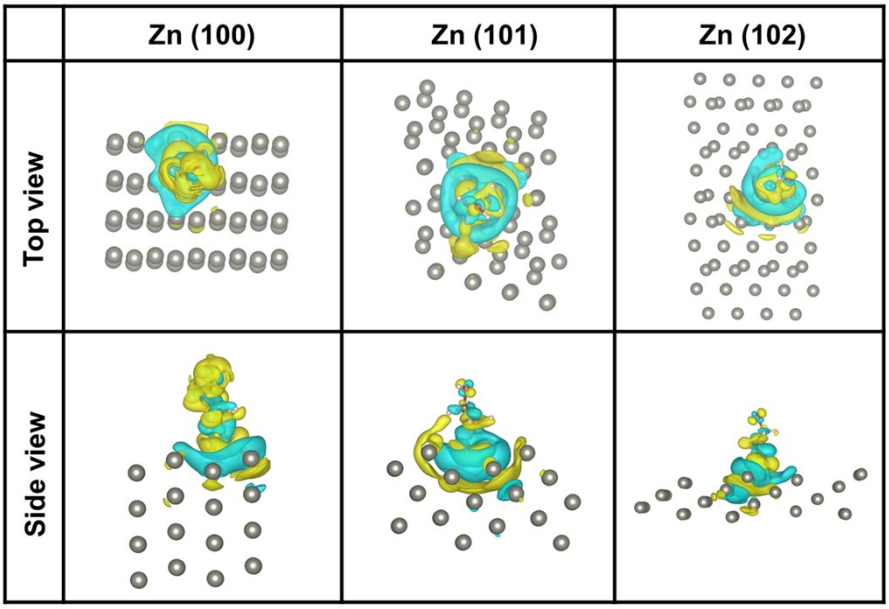

Figure S26. Differential charge density distribution of β-ME adsorbed on Zn (100), Zn (101) and Zn (102) crystal planes from side and top view.

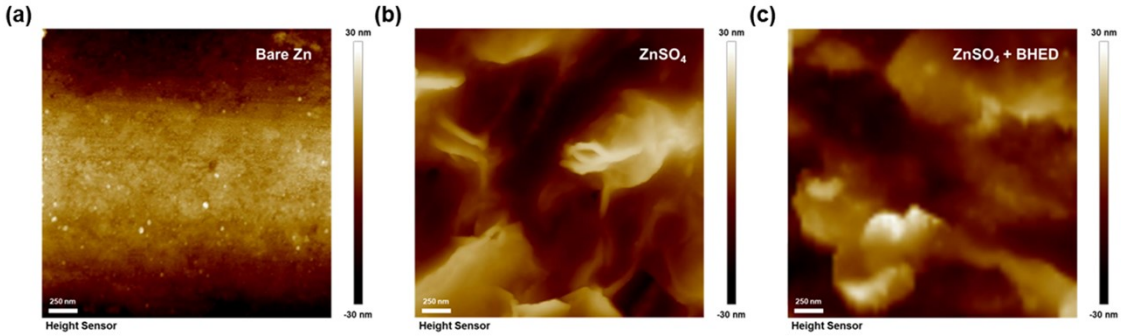

Figure S27. AFM images of a) bare Zn, and Zn foils after 10 cycles in b) $ZnSO_4$ and $ZnSO_4$ + BHED electrolytes at 1 mA cm^{-2} and 1 mA h cm^{-2}.

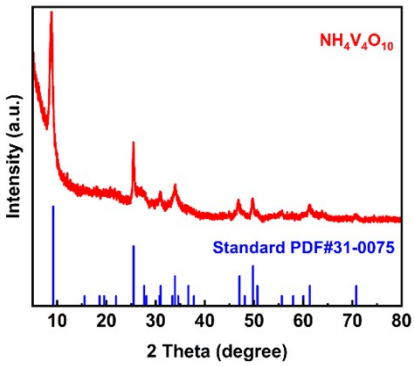

Figure S28. XRD pattern of the synthesized $NH_4V_4O_{10}$ cathode material.

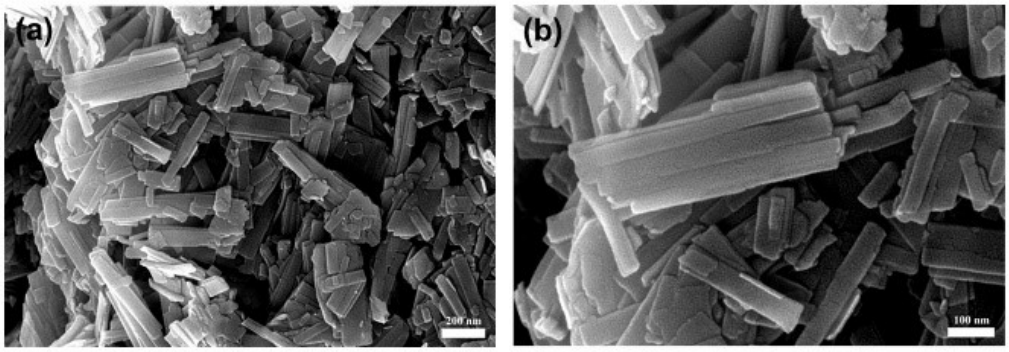

Figure S29. SEM images of the synthesized $NH_4V_4O_{10}$ cathode material.

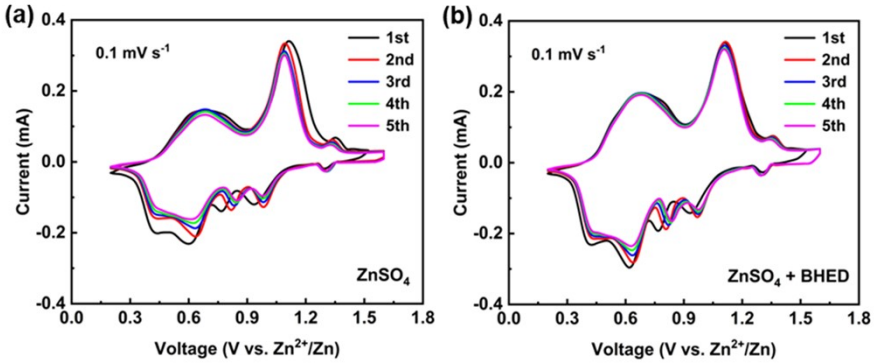

Figure S30. CV profiles of the Zn||NVO full cells in a) $ZnSO_4$ and b) $ZnSO_4$ + BHED electrolytes with a scan rate of 0.1 mV s^{-1}.

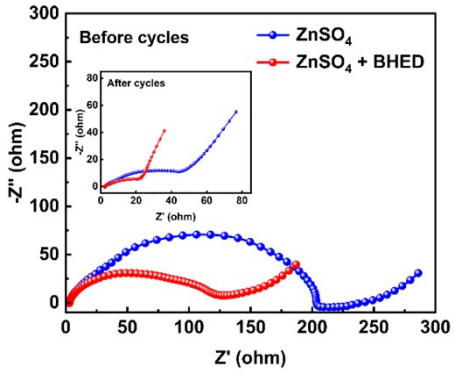

Figure S31. EIS plots of the Zn||NVO full cells in $ZnSO_4$ and $ZnSO_4$ + BHED electrolytes before and after cycling.

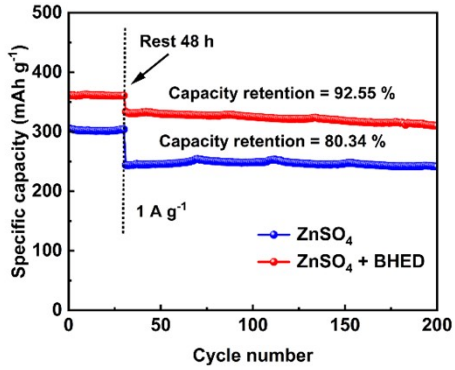

Figure S32. Cyclic performances after resting for 48 h of the Zn||NVO full cells in

$ZnSO_4$ and $ZnSO_4$ + BHED electrolytes at 1 A g^{-1}.

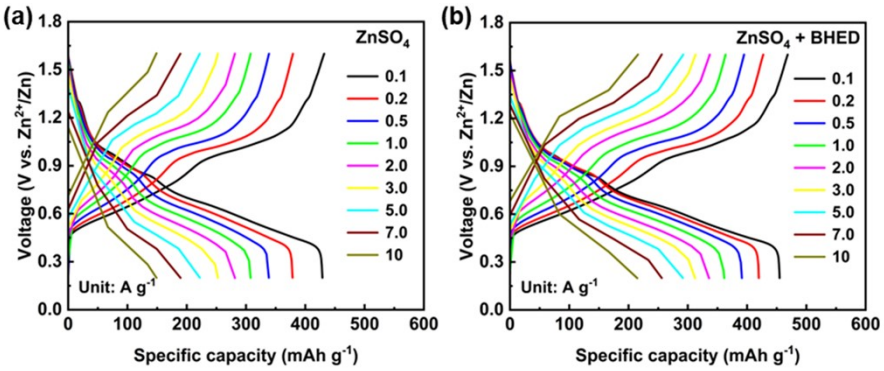

Figure S33. Charge-discharge curves of the Zn||NVO full cells in a) $ZnSO_4$ and b) $ZnSO_4$ + BHED electrolytes at various current densities.

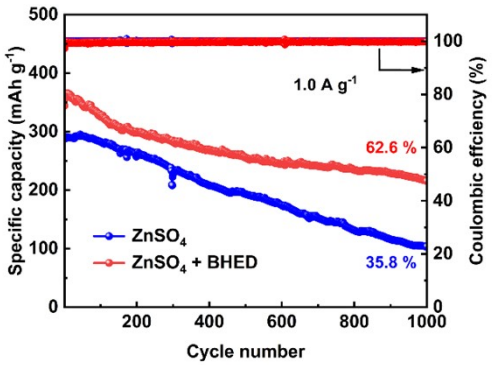

Figure S34. Cyclic performance of the Zn||NVO full cells in $ZnSO_4$ and $ZnSO_4$ + BHED electrolytes at 1.0 A g^{-1}.

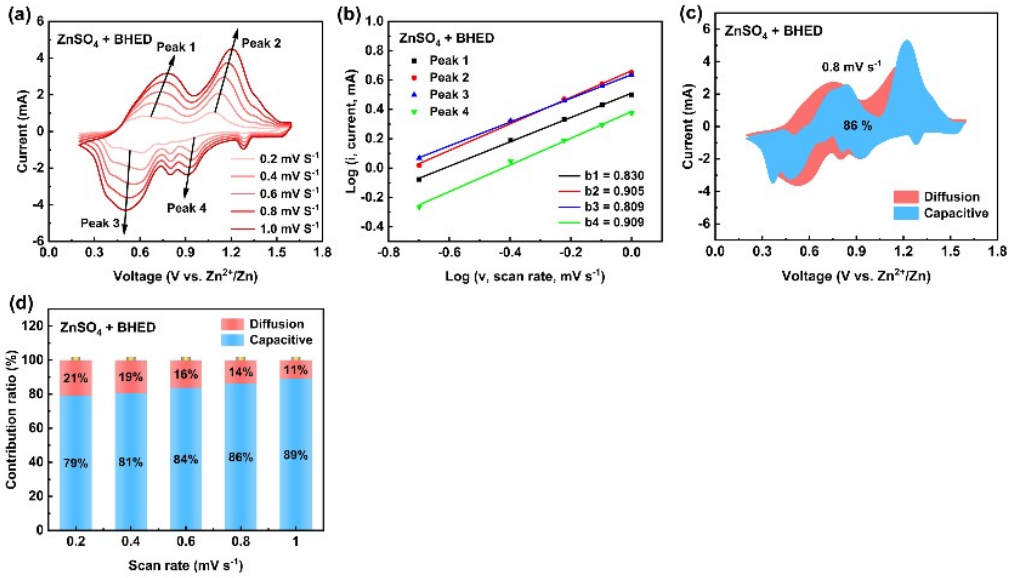

Figure S35. a) CV curves of the Zn||NVO full cells in $ZnSO_4$ + BHED electrolytes at the scan rates from 0.2 to 1 mV s^{-1}. b) Log (peak current) versus log (scan rate) plots for the b values. c) CV curves with capacitive and ionic diffusion contribution at 0.8 mV s^{-1}. d) The capacitive and ionic diffusion contribution at different scan rates.

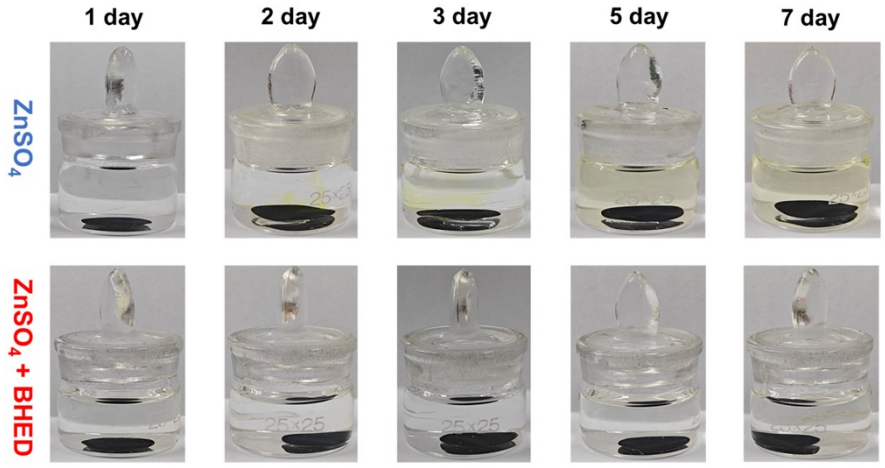

Figure S36. Digital photos of $NH_4V_4O_{10}$ cathodes soaked in $ZnSO_4$ and $ZnSO_4$ + BHED electrolytes for a week.

In Zn||$NH_4V_4O_{10}$ full batteries, the drastic capacity degradation is mainly attributed to the dissolution of the cathode material. Specifically, when the $NH_4V_4O_{10}$

cathode material is immersed in the electrolyte, its structure may be damaged due to dissolution, leading to the loss of active material and consequently a significant reduction in battery capacity. To verify the positive effect of the BHED additive on the $NH_4V_4O_{10}$ cathode, the $NH_4V_4O_{10}$ electrodes were immersed in 2M $ZnSO_4$ and 2M $ZnSO_4$ + BHED electrolytes, respectively, for one week. The results showed that the color of the $ZnSO_4$ electrolyte turned significantly yellow with time, indicating the gradual dissolution of $NH_4V_4O_{10}$; while the $ZnSO_4$ + BHED electrolyte always remained transparent. This color difference indicates that the addition of BHED effectively inhibits the dissolution of $NH_4V_4O_{10}$ and significantly enhances its stability in the $ZnSO_4$ electrolyte, thus reducing the capacity loss due to dissolution.[7-11]

Table S1. Comparison of lifespan of this work with previously reported the Zn||Zn symmetric cells.

Optimizing strategy	Modified electrolyte	Current density (mA cm^{-2})	Capacity density (mAh cm^{-2})	Lifespan (h)	Ref.
Electrolyte design	**2 M $ZnSO_4$ + 4 mM BHED**	**0.5**	**0.5**	**6300**	**This work**
Electrolyte design		**1**	**1**	**2000**	**This work**
Electrolyte design	2 M $ZnSO_4$ + 0.05 M NaDFOB	0.5	1	600	[10]
Electrolyte design	2 M $ZnSO_4$ + 3 vol % DGEM	0.5	0.25	3000	[9]
Electrolyte design	2 M $Zn(OTF)_2$ + TMS (TMS: H_2O = 1: 1)	1	1	1800	[12]
Electrolyte design	2 M $ZnSO_4$ + 15 vol% DMF	0.5	0.25	1970	[13]
Electrolyte design	2 M $Zn(OTf)_2$ + 10 mM HPA	0.5	0.5	3000	[14]
Electrolyte design	1 M $Zn(OAc)_2$ + FA (H_2O/FA = 1: 1, vol%)	0.5	0.25	860	[15]

Electrolyte design	2 M $ZnSO_4$ + 0.5 M $MnSO_4$ + 7 M Mu	1	1	800	[16]
Electrolyte design	1 M $ZnSO_4$ + 0.25 mM PA	2	1	1000	[17]
Electrolyte design	1 M $Zn(CF_3SO_3)_2$ + 45 wt% PEG	0.5	0.25	1500	[18]
Electrolyte design	2 M $ZnSO_4$ + 0.5 mM TMA_2SO_4	1	1	500	[19]
Electrolyte design	2 M $ZnSO_4$ + 1 g L^{-1} SDBS	0.2	0.2	1035	[20]
Electrolyte design	1 M $ZnSO_4$ + 500 mM Suc	0.5	0.5	3300	[21]
Electrolyte design	2 M $ZnSO_4$ + 0.25 M IU	1	0.5	1500	[22]
Electrolyte design	2 M $ZnSO_4$ + 50 vol% PG	0.5	0.5	3500	[23]
Electrolyte design	2 M $Zn(OTF)_2$ + 40 vol% DG	1	0.5	3500	[24]
Electrolyte design	2 M $ZnSO_4$ + 0.5 wt% DTPA-Na	0.5	0.5	4400	[25]

Electrolyte design	2 M $ZnSO_4$ + 0.5 g L^{-1} MPS	1	1	1000	[26]
Electrolyte design	1 M $Zn(CF_3SO_3)_2$ + 10 wt% ACN	1	1	1200	[6]

Table S2. Corrosion potential and corrosion current density in $ZnSO_4$ and $ZnSO_4$ + BHED electrolytes.

Symmetric cells	J_{corr} / (mA cm^{-2})	E_{corr} / mV	I / %
$ZnSO_4$	0.222	-15	-
$ZnSO_4$ + BHED	0.193	-7	13.1%

Table S3. EIS fitting results of the Zn||Zn symmetric cells in $ZnSO_4$ and $ZnSO_4$ + BHED electrolytes at different temperatures.

Symmetric cells	Resistance	30 °C	40 °C	50 °C	60 °C
$ZnSO_4$	R_{ct}	790	436.9	294.9	197.9
$ZnSO_4$ + BHED		248.7	194.7	163.3	109.9

Supporting Video

Video S1.mp4

Video S1. In-itu optical microscopy video of Zn^{2+} deposition on the Zn electrode surface in $ZnSO_4$ electrolyte.

Video S2.mp4

Video S2. In-itu optical microscopy video of Zn^{2+} deposition on the Zn electrode surface in $ZnSO_4$ + BHED electrolyte.

Video S3.mp4

Video S3. Three series-connected Zn||$NH_4V_4O_{10}$ flexible batteries with $ZnSO_4$ + BHED electrolyte power continuously 22 LED lights video.

Supporting references

1. L. Chen, H. Yue, Z. Zhang, Y. Ma, Y. Wang, M. Xu, Y. Huang and G. Yuan, Chem. Eng. J., 2023, 455, 140679.

2. Y. Wang, R. Zhao, M. Liu, J. Yang, A. Zhang, J. Yue, C. Wu and Y. Bai, Adv. Energy Mater., 2023, 13, 2302707.

3. S. Zhang, Q. Gou, W. Chen, H. Luo, R. Yuan, K. Wang, K. Hu, Z. Wang, C. Wang, R. Liu, Z. Zhang, Y. Lei, Y. Zheng, L. Wang, F. Wan, B. Li and M. Li, Adv. Sci., 2024, 11, 2404968.

4. X. Zhao, X. Zhang, N. Dong, M. Yan, F. Zhang, K. Mochizuki and H. Pan, Small, 2022, 18, 2200742.

5. H. Ren, S. Li, B. Wang, Y. Zhang, T. Wang, Q. Lv, X. Zhang, L. Wang, X. Han, F. Jin, C. Bao, P. Yan, N. Zhang, D. Wang, T. Cheng, H. Liu and S. Dou, Adv. Mater., 2023, 35, 2208237.

6. J. Zheng, B. Zhang, X. Chen, W. Hao, J. Yao, J. Li, Y. Gan, X. Wang, X. Liu, Z. Wu, Y. Liu, L. Lv, L. Tao, P. Liang, X. Ji, H. Wang and H. Wan, Nano-Micro Lett., (2024) 16:145.

7. F. Wan, L. Zhang, X. Dai, X. Wang, Z. Niu and J. Chen, Nat. Commun., (2018) 9:1656.

*8. Y. Li, P. Wu, W. Zhong, C. Xie, Y. Xie, Q. Zhang, D. Sun, Y. Tang and H. Wang, Energy Environ. Sci., 2021, **14**, 5563-5571.*

9. B. Xie, Q. Hu, X. Liao, X. Zhang, H. Lang, R. Zhao, Q. Zheng, Y. Huo, J. Zhao, D. Lin and X.-L. Wu, Adv. Funct. Mater., 2024, 34, 2311961.

10. Z. Wang, J. Diao, G. Henkelman and C. B. Mullins, Adv. Funct. Mater., 2024, 2314002.

11. Z. Wang, J. Diao, J. N. Burrow, Z. W. Brotherton, N. A. Lynd, G. Henkelman and C. B. Mullins, Adv. Funct. Mater., 2024, 34, 2311271.

12. Y. Zhong, X. Xie, Z. Zeng, B. Lu, G. Chen and J. Zhou, Angew. Chem., Int. Ed., 2023, 62, e202310577.

13. M. He, J. Chen, A. Hu, Z. Yan, L. Cao and J. Long, Energy Storage Mater., 62 (2023) 102941.

*14. Z. Yang, Y. Sun, S. Deng, H. Tong, M. Wu, X. Nie, Y. Su, G. He, Y. Zhang, J. Li and G. Chai, Energy Environ. Sci., 2024, **17**, 3443-3453.*

*15. C. You, R. Wu, X. Yuan, L. Liu, J. Ye, L. Fu, P. Han and Y. Wu, Energy Environ. Sci., 2023, **16**, 5096-5107.*

*16. Y. Deng, H. Wang, M. Fan, B. Zhan, L.-J. Zuo, C. Chen and L. Yan, J. Am. Chem. Soc., 2023, **145**, 20109-20120.*

*17. Y. Chen, F. Gong, W. Deng, H. Zhang and X. Wang, Energy Storage Mater., 2023, **58**, 20-29.*

18. Z. Cao, X. Zhu, S. Gao, D. Xu, Z. Wang, Z. Ye, L. Wang, B. Chen, L. Li, M. Ye and J. Shen, Small, 2022, 18, 2103345.

19. H. Cao, X. Huang, Y. Liu, Q. Hu, Q. Zheng, Y. Huo, F. Xie, J. Zhao and D. Lin, J. Colloid Interface Sci., 627 (2022) 367–374.

20. X. Yang, Q. Zhou, S. Wei, X. Guo, P. J. Chimtali, W. Xu, S. Chen, Y. Cao, P. Zhang, K. Zhu, H. Shou, Y. Wang, X. Wu, C. Wang and L. Song, Small Methods, 2023, 2301115.

21. L. Zhou, R. Yang, S. Xu, X. Lei, Y. Zheng, J. Wen, F. Zhang and Y. Tang, Angew. Chem., Int. Ed., 2023, 62, e202307880.

*22. X. Wang, Y. Ying, X. Li, S. Chen, G. Gao, H. Huang and L. Ma, Energy Environ. Sci., 2023, **16**, 4572-4583.*

23. J. Li, S. Zhou, Y. Chen, X. Meng, A. Azizi, Q. He, H. Li, L. Chen, C. Han and A. Pan, Adv. Funct. Mater., 2023, 2307201.

24. R. Wang, Q. Ma, L. Zhang, Z. Liu, J. Wan, J. Mao, H. Li, S. Zhang, J. Hao, L. Zhang and C. Zhang, Adv. Energy Mater., 2023, 13, 2302543.

25. Y. Huang, H. Yan, W. Liu and F. Kang, Angew. Chem., Int. Ed., 2024, 63, e202409642.

26. T. Wu, C. Hu, Q. Zhang, Z. Yang, G. Jin, Y. Li, Y. Tang, H. Li and H. Wang, Adv. Funct. Mater., 2024, 34, 2315716.